Power Flow Control of the Grid-Integrated Hybrid DG System using an ARFMF Optimization

Original Scientific Paper

Saleem Mohammad
Electrical and Electronics Engineering,
Sathyabhama Institute of Science & Technology
Chennai-119, India
saleem238@gmail.com

S.D Sundarsingh Jeebaseelan
Electrical and Electronics Engineering, Sathyabhama
Institute of Science & Technology
Chennai-119, India
Sundarsingh.eee@sathyabama.ac.in

Abstract *– A power flow control scheme for a grid-integrated Hybrid DG System (HDGS) is presented in this work, utilizing an advanced random forest algorithm combined with the moth-flame optimization (ARFMF) approach. The proposed control scheme combines the random forest algorithm (RFA) and moth-flame optimization algorithm (MFO) for consolidated execution. The random forest algorithm (RFA), an AI technique, is well-suited for nonlinear systems due to its accurate interpolation and extrapolation capabilities. It is an ensemble learning method that combines multiple decision trees to make predictions. The algorithm constructs a forest of decision trees and aggregates their predictions to produce the final output. The moth-flame optimization (MFO) process is a meta-heuristic optimization procedure inspired by the transverse orientation of moths in nature. It improves initial random solutions and converges to superior positions in the search area. Similarly, the MFO is effective in nonlinear systems as it accurately interpolates and extrapolates arbitrary information. In the proposed technique, the RFA performs the calculation process to determine precise control gains for the HDGS through online implementation based on power variation between the source side and the load side. The recommended dataset is used to implement the AI approach for online execution, reducing optimization process time. The learning process of the RFA is guided by the MFO optimization algorithm. The MFO technique defines the objective function using system information based on equal and unequal constraints, including the accessibility of renewable energy sources, power demand, and state of charge (SOC) of storage systems. Storage devices such as batteries stabilize the energy generated by renewable energy systems to maintain a constant, stable output power. The proposed model is implemented on the MATLAB/Simulink platform, and its execution is compared to previous approaches.*

Keywords*: moth-flame optimization, random forest algorithm, Microgrid, optimization, nonlinear systems*

1. INTRODUCTION

The evolution of the energy sector is being driven by the urgent need to address environmental issues and reduce reliance on fossil fuels for electricity generation. This shift towards sustainable energy sources requires the integration of innovative approaches to facilitate the transformation. As renewable energy sources and distributed generators become more prevalent, it is imperative to devise new strategies for effectively managing and operating the power grid. The objective is to ensure the consistent and high-quality delivery of electricity while maintaining or enhancing the reliability of the power supply. This entails the development of robust frameworks and technologies that can accommodate the increasing complexity and variability associated with renewable energy integration while upholding grid stability and performance. By leveraging innovation in grid management, we can pave the way for a sustainable and resilient energy future. [1]

The need for energy storage devices in the DC link arises from the growing adoption of renewable energy sources driven by the transition to clean and sustainable energy. However, renewable energy sources, such as solar (PV) and wind, are characterized by their variability and unpredictability. This variability poses challenges in effectively harnessing these energy sources, necessitating the use of energy storage devices to balance power and ensure a smooth and reliable power supply. [2]

Inverter reactive power compensation alone is insufficient to handle load variations, resulting in voltage sag, which can lead to operational issues [3]. To overcome this limitation, additional measures and strategies are required to effectively manage load variations and maintain stable voltage levels within the system. The complementarity and unpredictability of PV and wind energy further compound the challenges of effectively harnessing these energy sources [4]. Fluctuating PV irradiation and wind speed make it difficult to predict and optimize their power generation. However, technological advancements, such as the utilization of double-fed induction generators in wind turbine systems, enable multiple wind turbines to operate at variable speeds [5]. This flexibility allows for better control and regulation of the generator's torque, aligning it with the desired power factor or generator terminal voltage. This regulation takes into account various factors, including the availability of wind, PV, hydro, and energy storage devices, to optimize the overall system performance.

Achieving power flow balance and minimizing the impacts of atmospheric conditions in a hybrid generation system with multiple renewable energy sources is essential. Power flow balance ensures a consistent meeting of energy demand by the hybrid generation system. Balancing the power flow between renewable energy sources helps maintain a stable and reliable power supply, reducing the risk of blackouts or disruptions in the electrical grid. By achieving power flow balance, the hybrid generation system can optimize the utilization of renewable energy resources. During periods of high PV irradiation, more power can be generated from the PV source, while in times of high wind speed, the wind turbines can contribute a larger share of the power. This balanced approach maximizes the use of available resources and improves the overall efficiency of the system. Atmospheric conditions, such as variations in PV irradiance and wind speed, can significantly impact the power output of renewable energy sources. Effective management of these variations and balancing the power flow enables the hybrid generation system to minimize the negative impacts caused by fluctuations in atmospheric conditions. This reduction in sudden power output changes allows for better control and integration of renewable energy into the grid.

The proposed hybrid technique, referred to as ARFMF, combines the Random Forest Algorithm (RFA) and Moth Flame Optimization (MFO) algorithms for hybrid optimization. This proposal aims to achieve a balance in power flow and minimize impacts. The work is structured as follows: Section 2 provides a review of recent research, Section 3 discusses control strategies for Hybrid DG Systems, Section 4 presents the recommended ARFMF approach, Section 5 presents simulation results, and finally, Section 6 concludes the paper.

2. RECENT RESEARCH WORK

In their study, T. P. Kumar [6] put forward an optimal control strategy for Hybrid DG Systems (HDGS) that combines RNN and ANN with lighting search optimization, referred to as ANNLSA. To achieve optimal power flow management in Hybrid DG Systems (HDGS), a technique that balances real and reactive power involves a parallel connection of solar, wind, fuel cells, and batteries. The incorporation of solar and wind energy into an electric grid is examined, and the effectiveness of the compensation strategy of the DC-DC converter is evaluated using the ANNLSA technique. In optimising active power management, the Lightning Search Algorithm (LSA) is utilized, while optimal reactive power management is achieved using a Recurrent Neural Network (RNN). T. F. Shatter [7] introduced a system that integrates 3 renewable sources—solar, wind, and fuel cells—with the primary objective of controlling and maximising the productivity of the renewable sources. The primary aim of the PV, wind, and FC energy sources is to be efficiently controlled and operated. To attain MPPT for both solar and wind systems, Fuzzy Logic Control is employed, directing the peak power to a regulated DC voltage bus. This fixed voltage bus is responsible for powering the load, and any surplus energy is utilised for the electrolysis of water to produce hydrogen for fuel cells.

Tazvinga [8] put forward an ideal power management model for an HDGS designed for isolated applications. The system combines solar photovoltaic, diesel, and battery power, and a controlling strategy is implemented to regulate the power flow between system components to meet the varying load demands throughout the day. In the proposed model, the main objective is to meet the load demand while satisfying system constraints. To achieve this, the model aims to determine the optimal power flow while minimising fuel and battery wear costs. This is accomplished by taking into consideration the availability of photovoltaic power, the battery bank's state of charge, and the varying load demand. The optimal solutions are evaluated for two different scenarios: one where objectives have equal weight and another where a higher weight is given to battery wear. Giving a higher weight to battery wear leads to a noticeable rise in system operational costs, primarily due to increased usage of the diesel generator. In their research, N. Bizon [9] proposes a new Energy Management Unit (EMU) control strategy that relies on the LF approach. The EMU control strategy is designed to maintain a charge-sustaining mode for the Energy Storage System (ESS), effectively minimizing battery stack capacity when directly connected to the DC bus.

K. Venkatesan and colleagues [10] have presented an optimal control strategy for Hybrid DG Systems (HDGSs), which incorporate photovoltaic and wind turbine systems alongside energy storage. The aim of the presented optimal control strategy is to optimise power flow control in HDGSs. To achieve this, K. Venkatesan et al. [10] propose combining the Whale Optimization

Algorithm (WOA) with an Artificial Neural Network (ANN) to create a more effective and efficient control strategy. In the proposed optimal control strategy by K. Venkatesan et al. [10], the Whale Optimization Algorithm (WOA) is incorporated into the Artificial Neural Network (ANN) learning process to minimise the error in the objective function. This results in the development of the WOANN approach, which combines the WOA and ANN. The WOANN approach predicts control gain parameters for HDGS to regulate power flow, taking into account factors such as renewable energy availability, storage device charge levels, and load power demand. It accomplishes this by examining active and reactive power variation at the load side.

2.1. BACKGROUND OF THE RESEARCH WORK

It is evident that the energy management of Hybrid DG Systems with energy storage devices involves the integration of multiple renewable sources, such as PV and wind power generators, along with a diesel power generator. Determining the appropriate size of PV, wind, and diesel power plants is a complex task in energy management. While the use of a fuzzy logic controller for a wind turbine, PV, hydrogen, or battery HDGS in energy management has demonstrated improved results, it does not fully capture the unique characteristics of fuzzy systems theory. The complexity of the problem, the variability of renewable energy sources and load demand, and the interdependence among multiple variables all contribute to the difficulty of achieving optimal energy management in hybrid DG systems. To address this challenge, various traditional energy management strategies, such as fuzzy logic, neuro-fuzzy, and optimization algorithms, have been employed. However, the stochastic nature of the velocity equation in the Particle Swarm Optimization (PSO) algorithm makes it difficult to determine the global best value. The need for an integrated MG system arises to tackle this challenge. However, there are only a few existing works in literature that address this issue, highlighting the importance and motivation for the present research.

3. CONTROL METHODS OF HYBRID DG SYSTEM

The HDGS control structure is established through the implementation of the ARFMF technique, as depicted in Fig. 1. The HDGS comprises a wind turbine, photovoltaic (PV), fuel cell (FC), and battery, which together ensure the energy transmission of the DC bus. Dynamic optimal power flow management is used to determine the optimal load and grid parameters, and the electrical energy produced by the system is evaluated. A circuit diagram is provided to illustrate the control modules of the HDGS unit with a VSI-based design [11].

The power flow management and control modules of the HDGS unit are designed based on the load and grid operational modes. In the case of grid-connected mode, the HDGS unit's active and reactive output powers are regulated based on their respective reference values. Thus, the VSI-based control system must adopt the appropriate power control mode to ensure optimal performance.

To meet changing load demands, the power supplied by the main grid and HDGS must be adjusted accordingly. Effective regulation of power flow between the HDGS and the utility is necessary to keep a constant supply of active and reactive power, and a proper connection between the power from the main grid and the PV array is needed to meet the load demand, as shown in [12].

The DC-link and PCC must satisfy the power balance equation, as expressed in the following equation.

$$P_{hres}(t)=P_{windturbine}(t)+P_{photovoltaic}(t)+P_{FuelCell}(t)+P_{battery}(t) \quad (1)$$

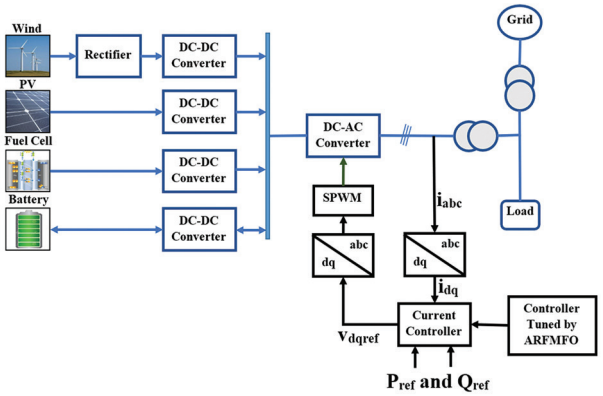

Fig. 1. Management Structure of HDGS with the Proposed Controller

Equation 1 is utilized to determine the power flow balance in the system, which accounts for the total power flow model. It involves calculating the power balance using the output from the HDGS and the demand from the load. PGRID (t) and PLOAD (t) are computed using equations 2 and 3, while QLOAD (t) and QGRID (t) are determined using equations 4 and 5.

$$P_{GRID}(t)=[P_{LOAD}(t)-P_{HRES}(t)] \quad (2)$$

$$P_{LOAD}(t)=[P_{HRES}(t)+P_{GRID}(t)] \quad (3)$$

$$Q_{GRID}(t)=[Q_{LOAD}(t)-Q_{HRES}(t)] \quad (4)$$

$$Q_{LOAD}(t)=[Q_{HRES}(t)+Q_{GRID}(t)] \quad (5)$$

The storage unit's battery power is determined by the discharge time as an energy source and the charging time as a load. However, due to the nonlinear variations in load demand and the uncertainty of renewable energy, it is challenging to maintain a consistent power balance [13]. To address this issue, a high-performance operation mode is necessary for effective power control in the HDGS unit. The measured values of active and reactive power are represented by Equations 6 and 7.

$$P_l(t)=3/2\,[v_d*i_d+v_q*i_q] \quad (6)$$

$$Q_l(t)=3/2\,[v_q*i_d+v_d*i_q] \quad (7)$$

Improvement of the current control scheme is necessary for better power tracking in the HDGS unit, as relying solely on it is insufficient to achieve high-performance operation.

3.1. CURRENT CONTROL STRATEGY

The power controller presented in Section 3.1 introduces two PI controllers to achieve controlled dynamic and reactive power to the load by controlling the power flow between the grid and the utility. Equations (8) and (9) illustrate the reference current for the control objective. The two PI controllers in the power controller communicate with the external control loop to generate the reference current vectors ID and IQ. Even a slight change in the reference current direction can ensure high-quality inverter output control, highlighting the attainment of the control objective.

$$i_d^*(t)=P_{error}(t)*(K_p^P+(K_p^P/S)) \quad (8)$$

$$i_q^*(t)=Q_{error}(t)*(K_p^Q+(K_p^Q/S)) \quad (9)$$

where $P_{error}(t)=[P_{ref}(t)-P_1(t)]$ and $Q_{error}(t)=[Q_{ref}(t)-Q_1(t)]$

The controller's output needs to be evaluated to ensure accurate tracking and minimize inverter drift. This is achieved by using two PI controllers to eliminate current error along with an inverter current feedback and grid voltage feedforward loop to enhance steady-state and dynamic performance. The PWM system is utilized by the controller to produce voltage vectors with reduced harmonic distortion. Equation (10) represents the transformation of Clarke's transformation equation into the stationary frame. In addition to the PWM system, the controller employs a current feedback loop and a grid voltage feedforward loop to enhance steady-state and dynamic performance, eliminate current error, and ensure accurate tracking while minimizing the drift of the inverter.

$$\begin{bmatrix} v_\alpha \\ v_\beta \\ v_0 \end{bmatrix} = \frac{2}{3}\begin{bmatrix} v_a \\ v_b \\ v_c \end{bmatrix}.\begin{bmatrix} 1 & -\frac{1}{2} & -\frac{1}{2} \\ 0 & \frac{\sqrt{3}}{2} & -\frac{\sqrt{3}}{2} \\ \frac{1}{2} & \frac{1}{2} & \frac{1}{2} \end{bmatrix} \quad (10)$$

In grid-connected mode, the HDGS unit regulates the amplitude and phase angle of the inverter current to provide the specified active and reactive power values to the grid. The control strategy for active and reactive power is based on frequency and voltage regulation. In figuring out how well the HDGS unit works, the outputs of the PV irradiance, wind turbine, and battery are considered. [15-17].

3.2. POWER CONTROL STRATEGY

The DC/DC converter of the HDGS unit is controlled by the PI controller to manage the grid power flow, as discussed in [18-20]. Real-time and reactive power optimization is performed using the controller parameters to achieve optimal power flow operations. The proposed technique generates optimal real and reactive power values for a three-phase grid-connected VSI system using the proposed controller.

3.3. PMSG WITH DC-DC CONVERTER

Wind power accessible from a wind turbine having a cross sectional area of A is

$$P_{wind}=1/2\ \rho A V_w^3 \quad (11)$$

The air density is denoted by ρ in kg/m^3 and the wind speed is represented by V_w in m/s.

Power coefficient C_p describes quantity of power obtainable after wind turbine for conversion is given as

$$P_w=C_p P_{wind} \quad (12)$$

Maximum value of C_p is Betz limit 0.593.

P_w is power extracted from rotor of the wind turbine given as

$$P_w=1/2\ \rho A V_w^3 C_p(\beta,\lambda) \quad (13)$$

λ is tip speed ratio given as

$$\lambda=(w_r R)/V_w \quad (14)$$

R is radius of rotor in m, w_r is rotor speed in rad/s, β is the pitch angle.

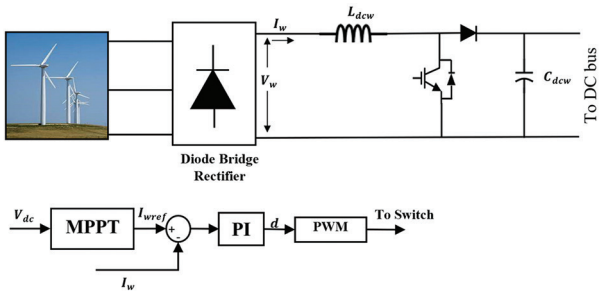

Fig. 2. PMSG based wind generation with DC-DC converter

Fig. 2 depicts a PMSG that is linked to the DC microgrid through a diode bridge rectifier and a DC-to-DC boost converter. The diagram also highlights the control procedure of the IGBT switch in the DC-to-DC converter. The MPPT is used to manage the reference inductor current Iwref generated from the rectifier to achieve maximum power from the wind generation system at a specific DC bus voltage V_{dc}.

PI controller in control system of DC-DC converter will administer duty cycle of switching pulses to be given to IGBT switch to maintain I_{wref} current through inductor. I_{wref} is the current determined by MPPT algorithm for a particular V_{dc}. Maximum power extraction from wind turbine can be possible at $(dP_w)/(dW_r)=0$, and as back emf is directly proportional to rotor speed hence

$$(dP_w)/(dV_{dc})=0 \quad (15)$$

The MPPT algorithm is used to determine the optimal value of the reference inductor current, Iwref, for a particular DC bus voltage, V_{dc}, to extract the maximum power from the PMSG. This involves adjusting the value of Iw based on the variation in the DC link voltage for a specific wind speed.

3.4. PV WITH MPPT BASED DC-DC CONVERTER

A DC-DC boost converter is employed to connect the PV panels to the DC microgrid, which utilizes an INC-based MPPT algorithm to operate at the maximum power point. The use of the MPPT algorithm helps to

extract the maximum amount of solar energy from the PV arrays by regulating the operating point. Fig. 4 illustrates the connection of the PV system to the DC bus through the DC-DC converter.

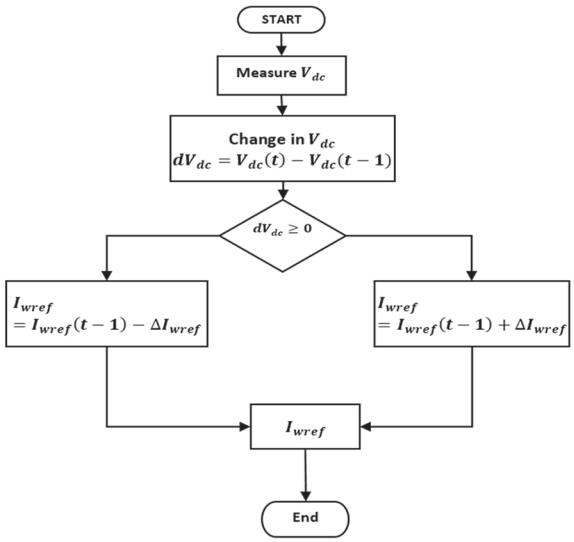

Fig. 3. Flow chart for MPPT algorithm of PMSG DC-DC converter

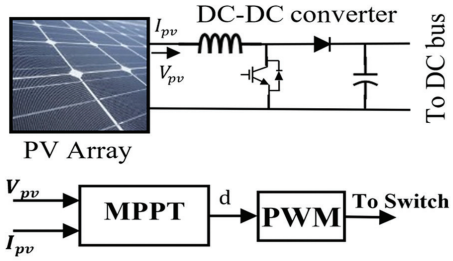

Fig. 4. PV with MPPT operated DC-DC converter

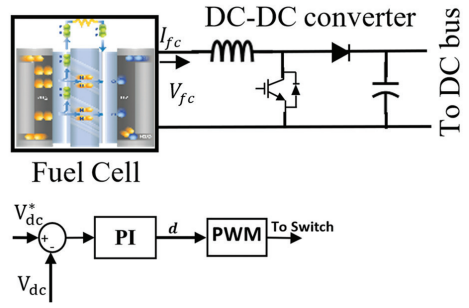

Fig. 5. FC system with DC-DC converter

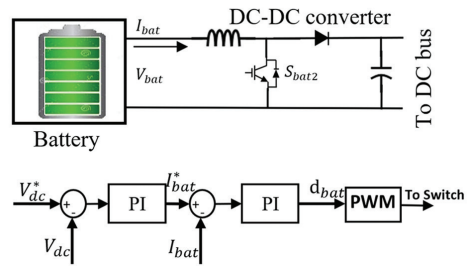

Fig. 6. Battery Storage system with DC-DC converter

Figs. 5 and 6 show the fuel cell system with DC converter and battery storage with DC converter.

4. PROPOSED APPROACH OF ARFMF

4.1. MOTH FLAME OPTIMIZATION ALGORITHM (MFO)

The Moth-Flame Optimization Algorithm is a metaheuristic optimization technique that imitates the navigation behavior of moths in low-light conditions using a mechanism called transverse orientation. This algorithm is inspired by the behavior of over 160,000 moth species found in nature. Moths have a two-stage life cycle consisting of the larval and adult stages.

Step 1: Parameter set

A parameter defines the operation of a system and is a constant value in an equation. Parameters are not limited to mathematical equations, as any system can have parameters that set its boundaries and conditions.

Step 2: Population Initialization

In the Moth-Flame Optimization Algorithm, moths serve as potential solutions for a given problem, with their positions representing the parameters of the problem. These moths can move through spaces of different dimensions, including 1-D, 2-D, 3-D, or even hyper-dimensional spaces, by exchanging their position vectors.

Step 3: Fitness Function

The fitness function determines the quality of a single solution in a population by evaluating its performance. At each iteration's end, to evaluate the effectiveness of the search process in the Moth-Flame Optimization Algorithm, the fitness value of each agent is computed. This fitness value serves as a measure of the quality of the search conducted by the agent.

Step 4: Optimal Selection

The positions of the moths are adjusted in relation to the best solutions they've encountered so far, which they do by flying in hyperspheres around them. The pattern of the flames, used as reference points, changes in each iteration based on the best solutions, causing the moths to update their positions accordingly [21-23].

4.2. RANDOM FOREST ALGORITHM (ARF)

Random subspace selection, a technique used in the design of random forests, helps forests of trees maintain accuracy as they grow without overtraining by restricting the trees to randomly selected feature dimensions [24].

To use the trained random forest algorithm for prediction, we need to apply the rules of each of the 100 random decision trees to the test features [25-29].

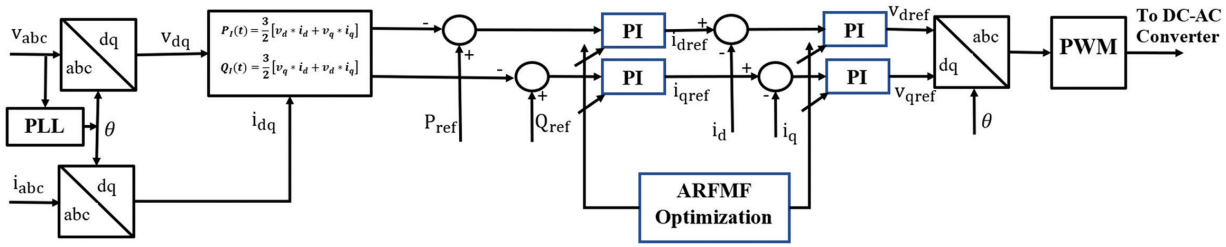

Fig. 7. Controlling Strategy of DC-AC Converter

The random forest algorithm calculates a predicted target by considering the votes of each unique target predicted by the 100 random decision trees. The votes of each target (e.g., x, y, and z) are determined by counting the number of trees that predict that target. For example, if 60 of the 100 decision trees predict target x, then x is returned as the final prediction of the random forest [30-32].

The following are the steps involved in RFA algorithm.

Step 1: Data Preparation

The algorithm begins by preparing the training data, which consists of input features (available power, load demand and control gains) and their corresponding target values (error between actual and reference values). Each sample in the training data contains a set of features and a known target value.

Step 2: Random Sampling

Random Forest uses a technique called bootstrap aggregating, or "bagging," to create multiple subsets of the training data. Each subset is obtained by sampling with replacement from the original data. This process creates different training sets, each potentially containing duplicate samples.

Step 3: Building Decision Trees

For each subset of the data, a decision tree is constructed. Decision trees are built using various algorithms, such as CART (Classification and Regression Trees). During the tree-building process, at each node, the algorithm selects the best feature to split the data based on certain criteria, typically the Gini impurity or information gain.

Step 4: Random Feature Selection

One of the distinguishing characteristics of Random Forest is that it randomly selects a subset of features at each node when building each decision tree. This random feature selection helps to introduce diversity among the trees and prevent overfitting by reducing the correlation between the trees.

Step 5: Tree Construction

The decision trees are constructed recursively by partitioning the data based on the selected features until reaching leaf nodes. Each leaf node represents a class label in the case of classification or a predicted value in the case of regression.

Step 6: Aggregating Predictions

Once the ensemble of decision trees is built, predictions are made by aggregating the individual predictions of each tree. For classification tasks, the class with many votes among the trees is chosen as the final prediction. For regression tasks, the average of the predicted values from all trees is taken.

Step 7: Evaluation and Generalization:

The performance of the Random Forest model is evaluated using evaluation metrics specific to the task at hand, such as accuracy, precision, recall, or mean squared error. The model's ability to generalize to unseen data is assessed using cross-validation or separate test datasets.

5. RESULT AND DISCUSSION

This section presents a discussion on the outcomes achieved by applying the proposed techniques in three distinct test cases, accompanied by a comparison with various existing techniques. The effectiveness of the proposed approach is emphasized by comparing its results to those obtained through the implementation of existing techniques in the MATLAB/Simulink platform. The main goal of the proposed method is to minimize power generation deviation and optimize the flow of active and reactive power in the Hybrid Distributed Generation System (HDGS) unit. The control strategy of the proposed technique is depicted in Fig. 7.

To assess the efficiency of the suggested system, it underwent testing with two specific scenarios: changes in irradiance and changes in load. The outcomes obtained from these tests were then compared to the results obtained using other techniques, namely MFO, LSA, and BAT optimization.

The system comprises various renewable energy sources, including Photovoltaic (PV) panels, wind turbines, Fuel Cells (FC), and batteries. To evaluate the effectiveness of the proposed method, it was subjected to three separate analytical cases, each representing a distinct set of conditions or parameters. These cases were designed to comprehensively assess the system's performance and measure its capabilities in handling different situations related to renewable energy generation and load management.

Table 1. Parameters of the System

PV Array	
Series connected modules	5
Parallel Strings	44
Maximum Power of Module	305 W
Open Circuit Voltage (V_oc)	64.2 V
Short Circuit Current (I_sc)	5.96 A
MPP voltage (V_mpp)	54.7 V
MPP Current (I_mpp)	5.58 A
Wind Turbine and PMSG	
Base Wind Speed	8 m/s
Nominal mechanical output power	50 kW
PMSG Stator Resistance and Inductance	0.425 ohm and 8.5 mH
Torque constant and inertia	3.2475 and 0.01197 kg.m2
Fuel Cell	
Power and Voltage	6 kW and 45 Vdc
Battery	
Nominal Voltage	100 V
Rated Capacity	60 Ah

- **Case 1:** Unbalanced source along with balanced load with PV Irradiance Pattern 1
- **Case 2:** Stable source along with unbalanced load with PV Irradiance pattern 2
- **Case 3:** Supply in balance with an unbalanced load.

An analysis was conducted on a case involving actual and volatile control limits in a microgrid system using existing methods such as MFO, LSA, and BAT, along with the proposed technique. The results obtained from the proposed technique were found to be optimal, and their significance is explained in detail below.

Case 1: Distorted supply with balanced load with PV Irradiance Pattern 1

In Case 1, conducted an analysis of the Hybrid Distributed Generation System (HDGS) under the conditions of unbalanced PV power supply and a balanced load. Throughout the analysis, the load power remained constant, while the PV power and wind speed were subject to variation. To illustrate this, Figs. 8(a) and 8(b) were utilized to showcase the analyses of PV irradiance and wind speed, respectively. In Fig. 8(a), the analysis of PV irradiance is given. The PV power output initiates at 1000 w/m2 and remains constant from 0 to 0.6 seconds, reflecting specific irradiation conditions. However, at 0.75 seconds, there is a sudden drop in PV irradiance, leading to a reduction in PV power output to 500 w/m2. This change in irradiation conditions significantly impacts the performance of the HDGS.

Fig. 8(b) represents the wind speed, which remains constant at 8 m/s throughout the analyzed time. Figs. 9(a) to 9(d) present a comparative analysis of PV, wind, Fuel Cell (FC), and battery power. The performance of the proposed ARFMF method is compared to existing methods such as MFO, LSA, and BAT.

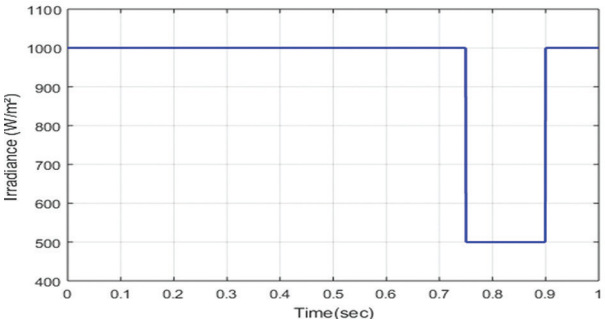

(a)

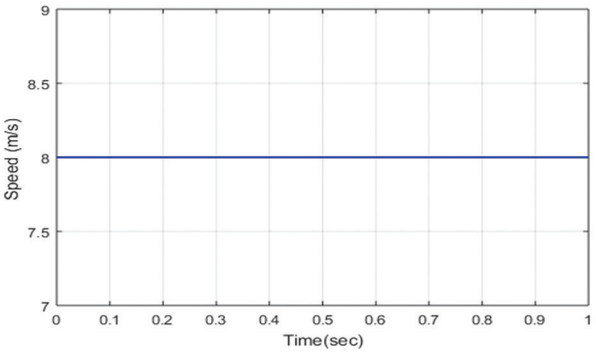

(b)

Fig. 8. Input Data to PV and wind (a) Solar Irradiance profile (b) Wind speed profile

In Fig. 9(a), the analysis focuses on PV power. It shows that the peak PV power of 5000 W is attained between 0.21 and 0.75 seconds. However, there is a reduction in PV power to 1100 W between 0.75 and 0.9 seconds, followed by a rise back up to 5000 W between 0.9 and 1 second. This fluctuation in PV power output demonstrates the dynamic nature of the system and the ability of the proposed ARFMF method to adapt to changing conditions and optimize power generation.

Fig. 9(b) presents the performance of the wind generation system. It achieves a maximum power output of 3300 kW, surpassing the performance of existing techniques such as MFO, LSA, and BAT. This comparison highlights the superior performance of the proposed ARFMF method in harnessing wind energy and maximizing power generation. The performance of the Fuel Cell (FC) power is depicted in Fig. 9(c). The analysis shows a maximum power output of 2503 W between 0.3 and 1 second. The proposed ARFMF method outperforms the existing techniques in terms of FC power generation, further emphasizing its effectiveness in optimizing power production from different sources within the HDGS.

Fig. 9(d) illustrates a comparison between the proposed and existing battery power methods. The ARFMF approach achieves a maximum battery power of 7000 W between 0.7 and 1 second, outperforming the other techniques. This result indicates that the proposed method is capable of effectively managing and utilizing battery storage to optimize power flow within the HDGS.

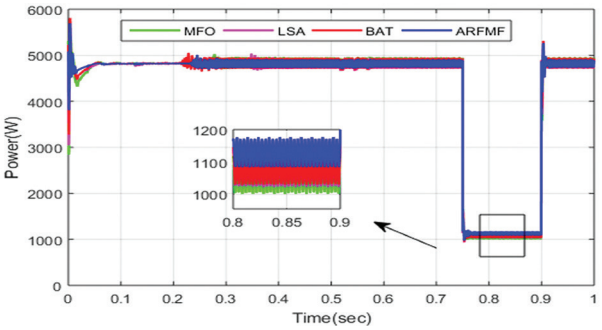

(a)

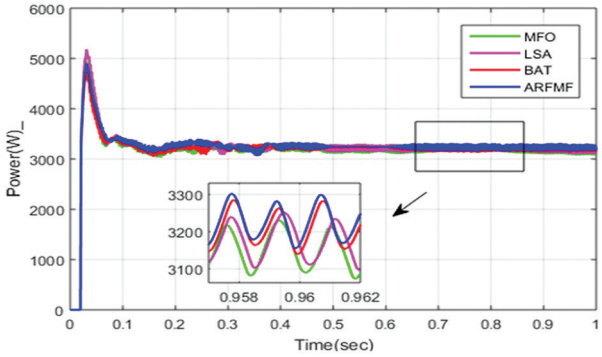

(b)

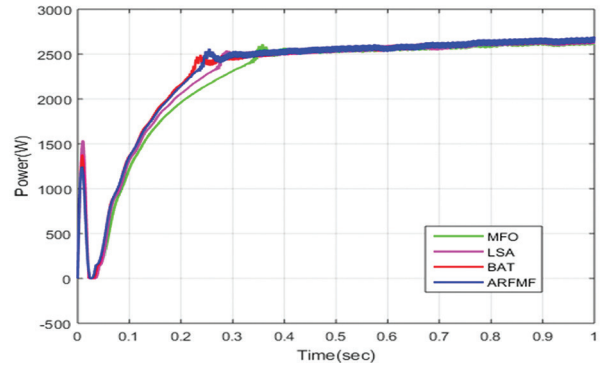

(c)

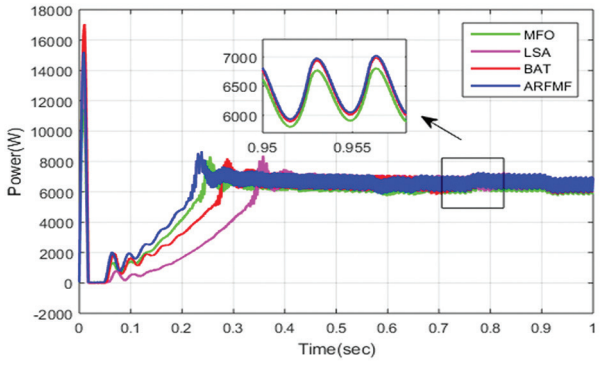

(d)

Fig 9. Power Comparison of (a) PV (b) wind (c) FC (d) Battery

Figs. 10(a) to 10(d) present a comparison of grid power, load power, total power, and fitness between the proposed ARFMF method and existing techniques.

In Fig. 10(a), the analysis compares the grid power achieved by the proposed ARFMF method with that of existing techniques. It is observed that the proposed method achieves the highest grid power of 4450 W between 0.8 and 1 second, surpassing the performance of the existing techniques. Fig. 10(b) focuses on the comparison of load power. The proposed ARFMF method achieves the highest load power of 20 kW between 0.3 and 1 second, outperforming the existing techniques. The total power analysis is depicted in Fig. 10(c). It shows the overall power output, considering all the generation sources in the HDGS. The analysis reveals that the total power starts at 0.5 kW at time 0 and increases to 2.4 kW. It then drops to 0.5 kW again from 2.4 kW, followed by a rise back to 2.4 kW. Between 0.75 and 0.9 seconds, there is a temporary decrease in total power due to a decrease in irradiance. Finally, the total power rises back to 2.4 kW. Fig. 10(d) illustrates the comparison of fitness between the proposed ARFMF method and existing techniques. Fitness represents the measure of how well a solution meets the desired objectives. The analysis reveals that the proposed technique achieves convergence at 17 iterations, outperforming the existing methods. The MFO technique converges at 20 iterations, LSA at 18 iterations, and BAT at 19 iterations.

In summary, Fig. 10(a) to 10(d) provide a comprehensive comparison of grid power, load power, total power, and fitness between the proposed ARFMF method and existing techniques. The findings emphasize the superior performance of the proposed method in terms of power generation, load fulfillment, overall power optimization, and convergence speed. These results validate the effectiveness and efficiency of the proposed ARFMF method in managing and optimizing power generation in the HDGS.

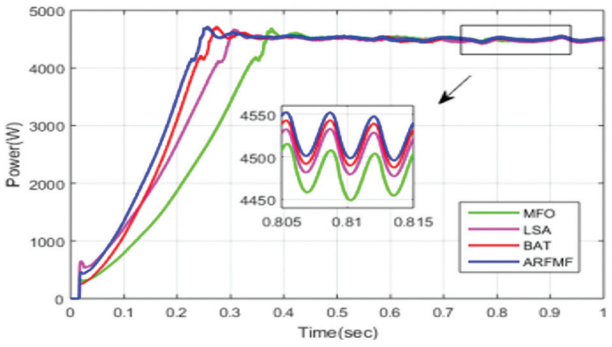

(a)

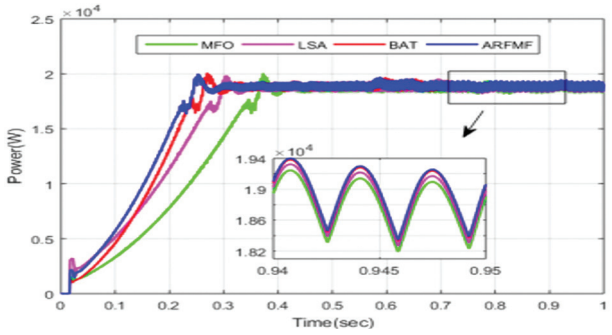

(b)

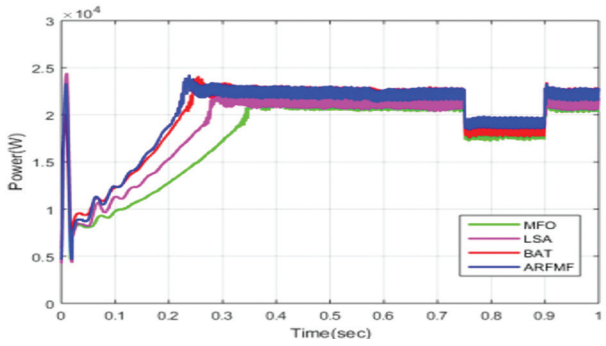

(c)

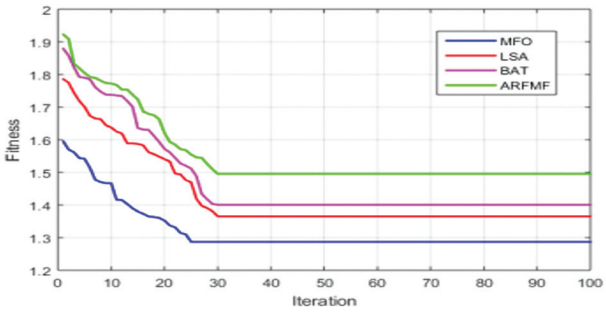

(d)

Fig 10. Evaluation assessment of (a) Grid power (b) Load power (c) Total power (d) Fitness

Case 2: Balanced supply with unbalanced load with PV irradiance pattern 2

In Case 2, the HDGS unit is analysed with an unbalanced PV power supply and a balanced load under the second pattern of PV irradiance. In this scenario, the load power remains constant while the PV power changes, and the wind speed is constant. The analyses of PV irradiance and wind speed are shown in Figs. 11(a) and 11(b), respectively. In Fig. 11(a), the PV irradiation is 1000w/m2 from 0 to 0.7 seconds then suddenly dropped to 0 w/m2 from 0.75 to 1 second. Throughout the analysis, wind speed is constant at 8 m/s as shown in Fig. 11(b).

Figs. 12(a) to 12(d) showcase the power generated from PV, wind, Fuel Cell (FC), and battery, comparing the proposed ARFMF technique with existing methods such as MFO, LSA, and BAT. In Fig. 12(a), the analysis focuses on the power generated from PV. It demonstrates that the peak PV power of 5000 watts occurs between 0.21 and 0.7 seconds. From 0.75 to 1 second, the PV power decreases and remains constant, as indicated in the figure.

Fig. 12(b) illustrates the power generated from the wind source. The proposed ARFMF technique achieves a higher wind power of 3300 watts between 0.878 and 0.882 seconds compared to the existing methods. The performance of FC power is depicted in Fig. 12(c). The proposed ARFMF method delivers a maximum power output of 2503 watts between 0.3 and 1 second, outperforming the existing techniques. Lastly, Fig. 12(d) presents a comparison between the proposed ARFMF technique and existing methods for battery power. The proposed technique achieves a maximum battery power of 1600 watts between 0.3 and 1 second.

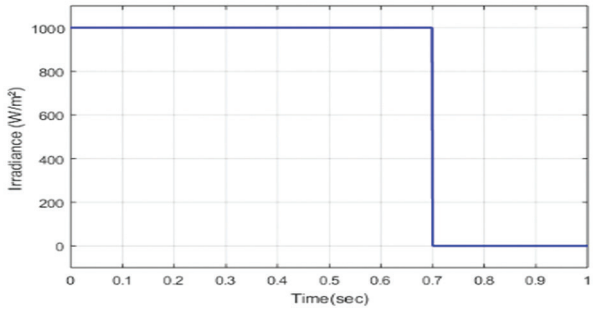

(a)

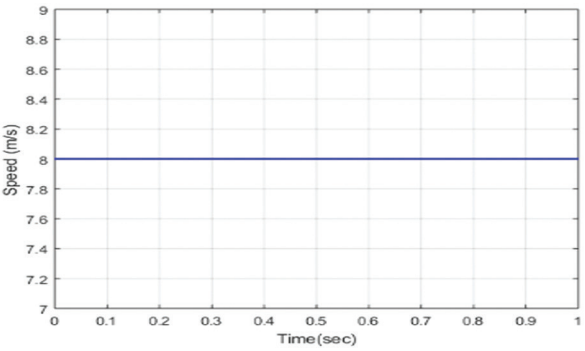

(b)

Fig. 11. Input Data to PV and wind (a) Solar Irradiance profile (b) Wind speed profile

Overall, the analysis in Figs. 12(a) to 12(d) underscores the superior performance of the proposed ARFMF technique in generating power from PV, wind, FC, and battery sources. These findings highlight the efficiency and effectiveness of the proposed technique in optimizing power generation and maximizing the output from different sources, outperforming the existing methods.

Figs. 13(a) to 13(d) provide a comparative analysis of grid power, load power, total power, and fitness between the proposed ARFMF technique and existing methods. In Fig. 13(a), the analysis focuses on grid power and compares the performance of the proposed ARFMF technique with existing methods. It is observed that the highest grid power of 4450W, achieved by the ARFMF technique, is observed between 0.8 and 0.81 seconds. Fig. 13(b) presents the assessment of load power, comparing the proposed ARFMF method with existing techniques. The highest load power of 20 kW, generated by the ARFMF method, occurs between 0.3 and 1 second. The analysis of total power is depicted in Fig. 13(c).

It shows the overall power output, considering all the generation sources in the system. The plot starts at 0.5 kW at time 0 seconds, then increases to 2.4 kW, followed by a decrease to 0.5 kW from 2.4 kW, and then a rise back to 2.4 kW. At 0.7 seconds, there is a decrease

in total power due to a decrease in irradiance. Fig. 13(d) compares the fitness of the proposed ARFMF technique with that of other methods. This result highlights the efficiency and effectiveness of the proposed ARFMF technique in finding optimal solutions and converging towards the desired objectives.

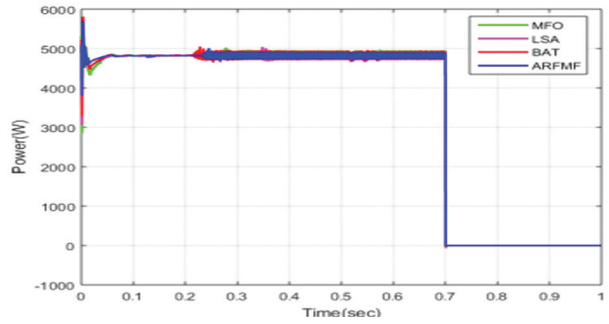

(a)

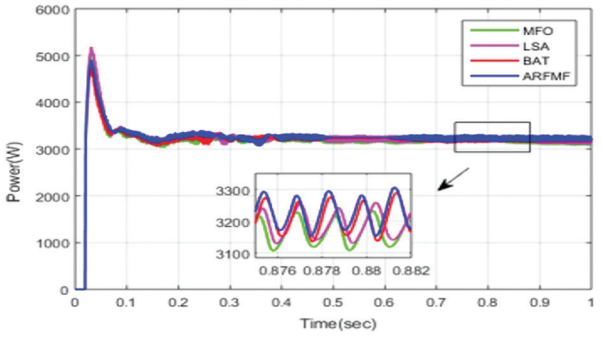

(b)

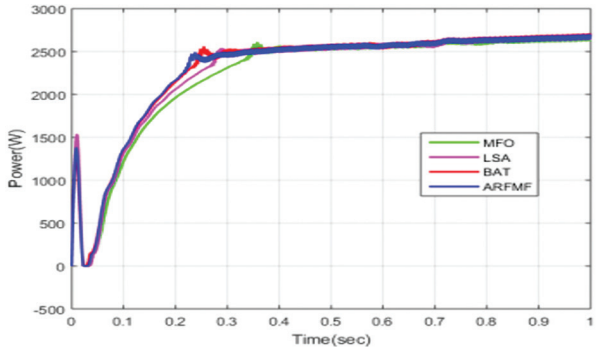

(c)

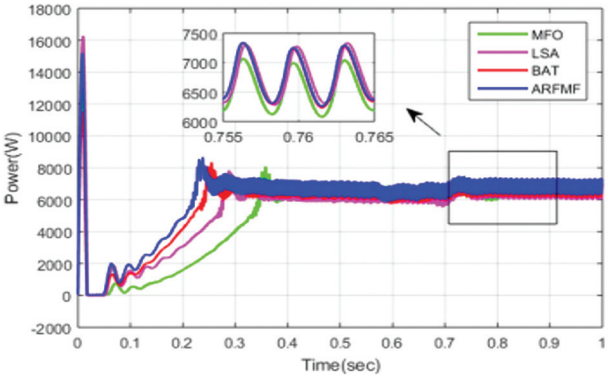

(d)

Fig. 12. Power Evaluation of (a) PV (b) wind (c) FC (d) Battery

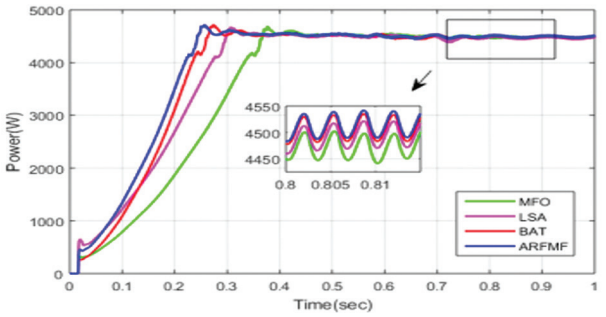

(a)

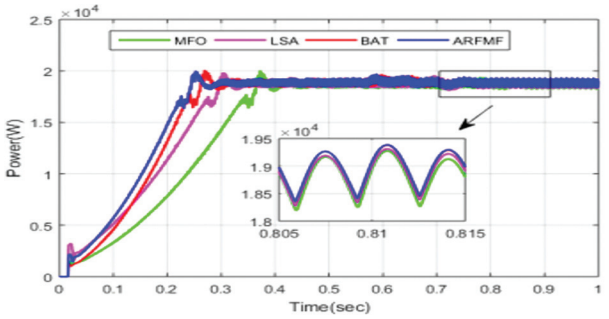

(b)

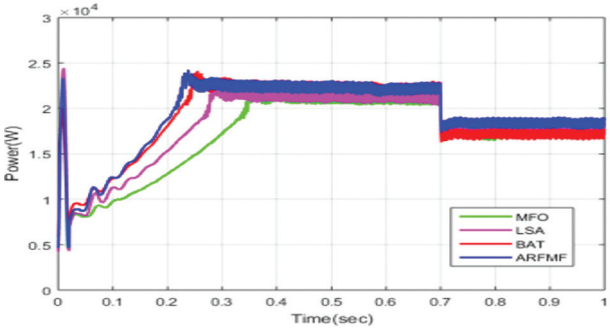

(c)

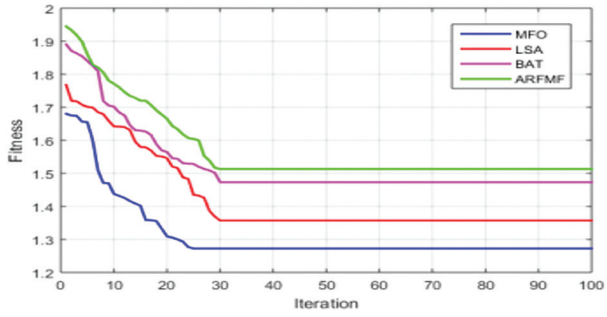

(d)

Fig. 13. Evaluation of (a) Grid power (b) Load power (c) Total power (d) Fitness

Case 3: Balanced supply with unbalanced load

Case 3 examines the HDGS under a balanced PV power supply, and in this scenario, an unbalanced load condition is considered where the load power is kept constant, while the PV power and wind speed are varied. Figs. 14(a) and 14(b) depict the analysis of PV irradiance and wind speed, respectively. As shown in Fig. 14(a), the irradiance remains constant from 0 to 1 second. Mean-

while, Fig. 14(b) shows that the wind speed remains constant at 8 m/s throughout the analysis.

Fig. 15(a) presents a comparison of PV power performance between the proposed ARFMF method and existing methods, including MFO, LSA, and BAT. The proposed method achieves a maximum PV power of 3800 W between 0.5 and 0.9 seconds, surpassing the power outputs of the other techniques. Between 0.25 and 1 second, the highest PV power of 5000 W is achieved.

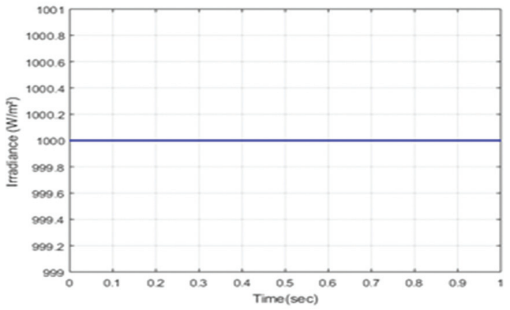

(a)

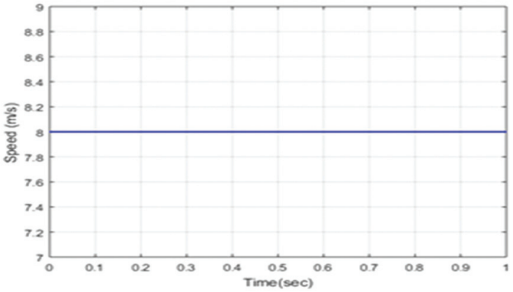

(b)

Fig. 14. Input Data to PV and wind (a) Solar Irradiance profile (b) Wind speed profile

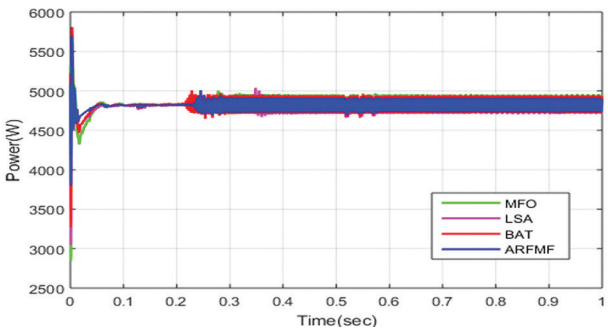

(a)

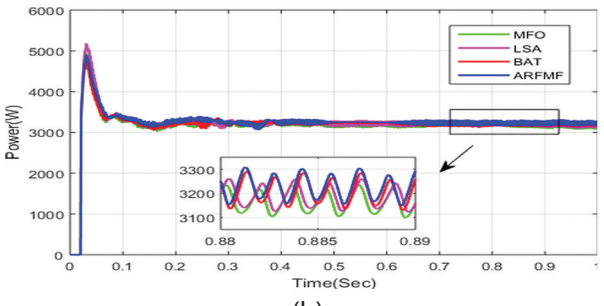

(b)

Fig. 15. Power Comparison of (a) PV (b) wind

Notably, the PV power decreases from 0.75 to 0.9 seconds and then rises again to 5000 W from 0.9 to 1 second. Fig. 16(a) illustrates the performance of FC power. The proposed ARFMF technique outperforms existing methods, achieving the highest FC power of 2503 W between 0.2 and 1 second. Fig. 16(b) compares the battery power between the proposed ARFMF method and other techniques.

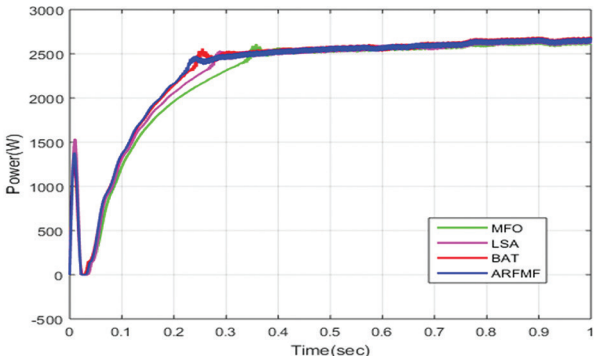

(a)

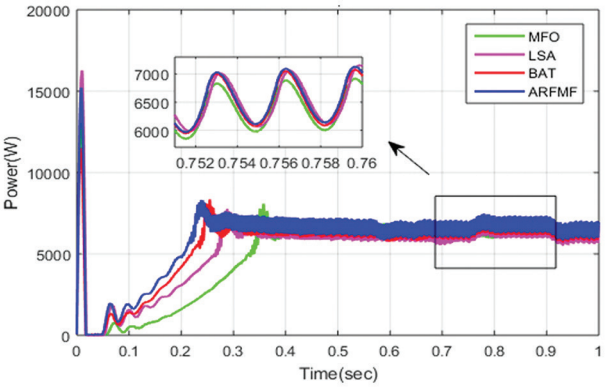

(b)

Fig. 16. Power Comparison of (a) FC (b) Battery

The ARFMF method generates the highest battery power of 7000 W between 0.7 and 1 second. In summary, Fig. 15(a) highlights the higher PV power achieved by the proposed ARFMF method compared to existing techniques, showcasing its effectiveness in adapting to changing conditions and optimizing PV power generation. Fig. 16(a) demonstrates the superior performance of the proposed technique in maximizing FC power output, and Fig. 16(b) highlights its ability to generate the highest battery power. These results validate the superiority of the proposed ARFMF method in optimizing power generation and overall system performance.

In Figs. 17(a)–17(b) and 18(a)-18(b) the comparison of grid power, load power, total power, and fitness is presented. Fig. 17(a) specifically shows the comparison of grid power between the proposed ARFMF technique and existing methods. The highest grid power of 4450W is achieved by the ARFMF method between 0.8 to 1 sec, making it the most powerful technique compared to others.

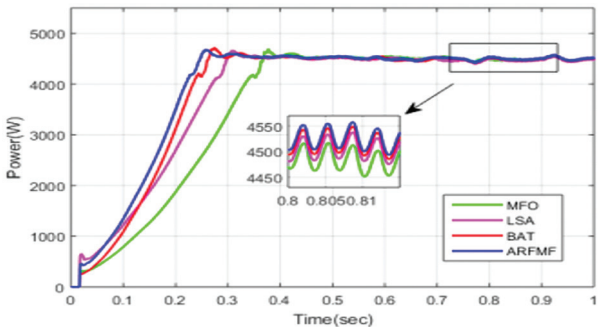

(a)

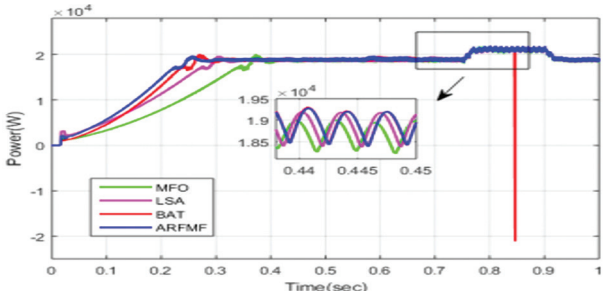

(b)

Fig. 17. Comparison of (a) Grid power (b) Load power

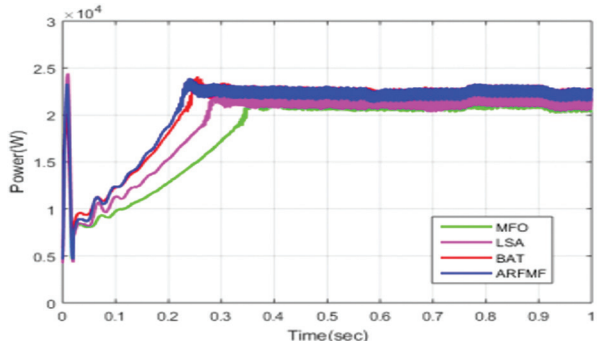

(a)

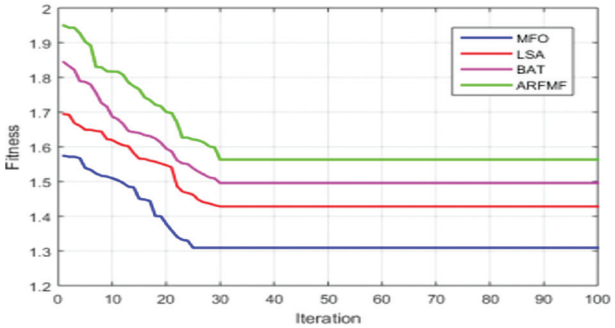

(b)

Fig. 18. Comparison of (a) Total power (b) Fitness

6. CONCLUSION

The paper proposes an energy management system for hybrid distributed generation systems (HDGS) that incorporates an energy storage device. The proposed model is implemented using the MATLAB/Simulink platform, and its performance is compared against existing methods. The energy system comprises various sources of renewable energy, including photovoltaic panels and wind generators, in addition to a diesel generator. The proposed energy management system faces challenges in determining the size of PV, wind, and diesel generators. It employs a combined approach using the Random Forest Algorithm (RFA) and Moth-Flame Optimization Algorithm (MFO). The effectiveness of this technique, called ARFMF, is evaluated under both balanced and unbalanced supply scenarios with changing loads. The proposed control scheme takes into account equal and unequal constraints, including the accessibility of renewable energy sources, power demand, and state of charge (SOC) of storage systems. By stabilizing the energy generated by renewable sources through storage devices such as batteries, the system maintains a constant and stable output power. The implementation of the proposed model on the MATLAB/Simulink platform demonstrates its efficacy compared to previous approaches. By utilizing an AI-based approach for online execution and reducing the optimization process time, the scheme enhances the efficiency and reliability of power flow control in the HDGS. The proposed controller's performance was compared with the MFO, LSA, and BAT techniques. The proposed model's accuracy, efficiency, and ability to handle nonlinear systems make it a valuable contribution to the field of power system control and optimization. The proposed control scheme should be further evaluated for its robustness and resilience against various system uncertainties, such as fluctuating renewable energy generation, varying load demands, and grid disturbances. Robust optimization techniques and advanced control strategies can be explored to enhance the system's ability to withstand and recover from such uncertainties while maintaining stable and reliable power supply.

7. REFERENCES:

[1] Y. Riffonneau, S. Bacha, F. Barruel, S. Ploix, "Optimal Power Flow Management for Grid Connected PV Systems With Batteries", IEEE Transactions on Sustainable Energy, Vol. 2, No. 3, 2011, pp. 309-320.

[2] G. Boukettaya, L. Krichen, "A dynamic power management strategy of a grid connected hybrid generation system using wind, photovoltaic and Flywheel Energy Storage System in residential applications", Energy, Vol. 71, 2014, pp. 148-159.

[3] K. Kusakana, "Optimal scheduled power flow for distributed photovoltaic/wind/diesel generators with battery storage system", IET Renewable Power Generation, Vol. 9, No. 8, 2015, pp. 916-924.

[4] S. Koko, K. Kusakana, H. Vermaak, "Optimal energy management of a grid-connected micro-hydroki-

netic with pumped hydro storage system", Journal of Energy Storage, Vol. 14, pp. 8-15, 2017

[5] N. Mbungu, R. Naidoo, R. Bansal, M. Bipath, "Optimisation of grid connected hybrid photovoltaic–wind–battery system using model predictive control design", IET Renewable Power Generation, Vol. 11, No. 14, 2017, pp. 1760-1768.

[6] T. Praveen Kumar, N. Subrahmanyam, M. Sydulu, "Power Flow Management of the Grid-Connected Hybrid Renewable Energy System: A PLSANN Control Approach", IETE Journal of Research, Vol. 67, No. 4, 2019, pp. 569-584.

[7] T. El-Shatter, M. Eskander, M. El-Hagry, "Energy flow and management of a hybrid wind/PV/fuel cell generation system", Energy Conversion and Management, Vol. 47, No. 9-10, 2006, pp. 1264-1280.

[8] H. Tazvinga, B. Zhu, X. Xia, "Optimal power flow management for distributed energy resources with batteries", Energy Conversion and Management, Vol. 102, 2015, pp. 104-110.

[9] N. Bizon, "Load-following mode control of a standalone renewable/fuel cell hybrid power source", Energy Conversion and Management, Vol. 77, 2014, pp. 763-772.

[10] K. Venkatesan, U. Govindarajan, "Optimal power flow control of hybrid renewable energy system with energy storage: A WOANN strategy", Journal of Renewable and Sustainable Energy, Vol. 11, No. 1, 2019, p. 015501.

[11] M. Kabir, Y. Mishra, G. Ledwich, Z. Dong, K. Wong, "Coordinated Control of Grid-Connected Photovoltaic Reactive Power and Battery Energy Storage Systems to Improve the Voltage Profile of a Residential Distribution Feeder", IEEE Transactions on Industrial Informatics, Vol. 10, No. 2, 2014, pp. 967-977.

[12] C. Bhattacharjee, B. Roy, "Advanced fuzzy power extraction control of wind energy conversion system for power quality improvement in a grid tied hybrid generation system", IET Generation, Transmission & Distribution, Vol. 10, No. 5, 2016, pp. 1179-1189.

[13] G. Mehta, S. Singh, "Power quality improvement through grid integration of renewable energy sources", IETE Journal of Research, Vol. 59, No. 3, 2013, p. 210.

[14] S. Dasgupta, S. Mohan, S. Sahoo, S. Panda, "Lyapunov Function-Based Current Controller to Control Active and Reactive Power Flow From a Renewable Energy Source to a Generalized Three-Phase Microgrid System", IEEE Transactions on Industrial Electronics, Vol. 60, No. 2, 2013, pp. 799-813.

[15] W. Al-Saedi, S. Lachowicz, D. Habibi, O. Bass, "Power flow control in grid-connected microgrid operation using Particle Swarm Optimization under variable load conditions", International Journal of Electrical Power & Energy Systems, Vol. 49, 2013, pp. 76-85.

[16] B. Daryanian, R. Bohn, "Sizing of electric thermal storage under real time pricing", IEEE Transactions on Power Systems, Vol. 8, No. 1, 1993, pp. 35-43.

[17] G. Wang, R. Wai, Y. Liao, "Design of backstepping power control for grid-side converter of voltage source converter-based high-voltage dc wind power generation system", IET Renewable Power Generation, Vol. 7, No. 2, 2013, pp. 118-133.

[18] X. Yuan, F. Wang, D. Boroyevich, Y. Li, R. Burgos, "DC-link Voltage Control of a Full Power Converter for Wind Generator Operating in Weak-Grid Systems", IEEE Transactions on Power Electronics, Vol. 24, No. 9, 2009, pp. 2178-2192.

[19] A. Roy, S. Kedare, S. Bandyopadhyay, "Optimum sizing of wind-battery systems incorporating resource uncertainty", Applied Energy, Vol. 87, No. 8, 2010, pp. 2712-2727.

[20] K. Ishaque, Z. Salam, A. Shamsudin, M. Amjad, "A direct control based maximum power point tracking method for photovoltaic system under partial shading conditions using particle swarm optimization algorithm", Applied Energy, Vol. 99, 2012, pp. 414-422.

[21] A. Garces, "A quadratic approximation for the optimal power flow in power distribution systems", Electric Power Systems Research, Vol. 130, 2016, pp. 222-229.

[22] A. Hermann, Q. Wu, S. Huang, A. Nielsen, "Convex Relaxation of Optimal Power Flow in Distribution Feeders with Embedded Solar Power", Energy Procedia, Vol. 100, 2016, pp. 43-49.

[23] M. Rouholamini, M. Mohammadian, "Heuristic-based power management of a grid-connected hy-

brid energy system combined with hydrogen storage", Renewable Energy, Vol. 96, 2016, pp. 354-365.

[24] A. Aktas, K. Erhan, S. Ozdemir, E. Ozdemir, "Experimental investigation of a new smart energy management algorithm for a hybrid energy storage system in smart grid applications", Electric Power Systems Research, Vol. 144, 2017, pp. 185-196.

[25] Y. Ueda, K. Kurokawa, T. Tanabe, K. Kitamura, H. Sugihara, "Analysis Results of Output Power Loss Due to the Grid Voltage Rise in Grid-Connected Photovoltaic Power Generation Systems", IEEE Transactions on Industrial Electronics, Vol. 55, No. 7, 2008, pp. 2744-2751.

[26] S. Ko, S. Lee, H. Dehbonei, C. Nayar, "Application of Voltage- and Current-Controlled Voltage Source Inverters for Distributed Generation Systems", IEEE Transactions on Energy Conversion, Vol. 21, No. 3, 2006, pp. 782-792.

[27] R. Kadri, J. Gaubert, G. Champenois, "An Improved Maximum Power Point Tracking for Photovoltaic Grid-Connected Inverter Based on Voltage-Oriented Control", IEEE Transactions on Industrial Electronics, Vol. 58, No. 1, 2011, pp. 66-75.

[28] Y. Luo, Y. Shi, Y. Zheng, N. Cai, "Reversible solid oxide fuel cell for natural gas/renewable hybrid power generation systems", Journal of Power Sources, Vol. 340, 2017, pp. 60-70.

[29] J. Allison, "Robust multi-objective control of hybrid renewable microgeneration systems with energy storage", Applied Thermal Engineering, Vol. 114, 2017, pp. 1498-1506.

[30] G. Kasal, B. Singh, "VSC with zigzag transformer based electronic load controller for a stand-alone power generation", International Journal of Power and Energy Conversion, Vol. 1, No. 1, 2009, p. 1.

[31] L. Ju, Z. Tan, J. Yuan, Q. Tan, H. Li, F. Dong, "A bi-level stochastic scheduling optimization model for a virtual power plant connected to a wind–photovoltaic–energy storage system considering the uncertainty and demand response", Applied Energy, Vol. 171, 2016, pp. 184-199.

[32] V. Das, S. Padmanaban, K. Venkitusamy, R. Selvamuthukumaran, F. Blaabjerg, P. Siano, "Recent advances and challenges of fuel cell based power system architectures and control – A review", Renewable and Sustainable Energy Reviews, Vol. 73, 2017, pp. 10-18.